PdxNby electrocatalysts for DEFC in alkaline medium: Stability, selectivity and mechanism for EOR

F. Moura Souza [a], J. Nandenha [b], B.L. Batista [a], V.H.A. Oliveira [a],
V.S. Pinheiro [a], L.S. Parreira [c], A.O. Neto [b], M.C. Santos [a,*]

[a] Laboratório de Eletroquímica e Materiais Nanoestruturados (LEMN), Centro de Ciências Naturais e Humanas
(CCNH), Universidade Federal do ABC (UFABC), Rua Santa Adélia 166, Bairro Bangu, 09210-170, Santo André, SP,
Brazil
[b] Instituto de Pesquisas Energéticas e Nucleares (IPEN), CNEN/SP, Avenida Prof. Lineu Prestes 2242, Cidade
Universitária, 05508-000, São Paulo, SP, Brazil
[c] Instituto de Química (IQ), Universidade de São Paulo (USP), Avenida Prof. Lineu Prestes 748, Cidade Universitária,
05508-000, São Paulo, SP, Brazil

ARTICLE INFO

ABSTRACT

Pd_xNb_y/C binary electrocatalysts supported on Vulcan carbon XC72 were prepared by the sol-gel method. The materials are characterized by transmission electron microscopy, X-ray diffraction analysis, inductively coupled plasma—mass spectrometry and contact angle measurements. The electrocatalytic activity for ethanol electrooxidation reaction was studied by cyclic voltammetry, chronoamperometry, Tafel slope and accelerated durability testing. The direct ethanol performance and the products after the experiments were studied by Fourier transform infrared spectroscopy. Pd_1Nb_1/C (50:50 wt%) shows superior activity for ethanol oxidation compared to the other electrocatalysts prepared in this work. All electrocatalysts containing Nb show the highest current exchange density. The Tafel slope results suggest that the Nb modified the Pd-electrocatalyst to obtain a reaction path with high selectivity with only a single determining step with low production of the intermediates for the ethanol oxidation reaction. The best performance is obtained using Pd_1Nb_1/C 18.11 mW cm^{-2}. The Pd_1Nb_1/C electrocatalyst displays the highest production of CO_2 and the lowest production of acetaldehyde. Pd_1Nb_1/C shows the highest peak current density during 1000 cycles of the experiment and the lowest mass loss of Pd after the cycling test. We find that the Nb modifies the Pd electrocatalysts from the bifunctional mechanism and reduces the loss of Pd during the accelerated durability test.

Introduction

Research has been conducted all over the world to provide technologies for the conversion of chemical energy into electric energy with reduced heat losses. Different types of fuel cells have been developed and investigated as promising technologies for such energy conversion. A direct liquid fuel cell (DLFC) has great potential because it does not require fuel

reforming or an ultrapure gas tank. In addition, it is compact and suitable for mobile applications.

DLFCs are divided into specific fuel cell (FC) subgroups, for example, direct ethanol fuel cells (DEFCs), which use ethanol as fuel at the anode and the existing oxygen from the atmospheric air at the cathode. These devices are ideal for portable applications such as electronic device chargers because they operate at room temperature and are easy to manipulate [1].

Ethanol has numerous advantages compared to other alcohols such methanol, which is more toxic and volatile [2,3]. Ethanol exhibits easy handling compared to glycerol and ethylene glycol [4]. In addition, ethanol can be produced from a renewable source (biomass) such as maize or sugarcane crops [5–7].

Furthermore, the ethanol oxidation reaction (EOR) that provides $12e^-$ per molecule in the complete reaction is a goal that still remains to be achieved. This difficulty is due the cleavage of the C–C bonds for the oxidation of ethanol to CO_2, which requires selective anode catalysts [5–7]. Therefore, the main intermediates of this reaction are acetaldehyde and acetate in the alkaline medium [8,9].

Palladium (Pd) has been shown to be the best catalytic metal for ethanol oxidation reaction (EOR) in alkaline medium for fuel cells. This metal shows a high power density per mg of catalytic metal [10]. However, the cost of Pd is too high to be commercially employed in these devices [10]. In addition, intermediate products formed from the EOR, for example, CO, poisoning the Pd surface and hindering the ethanol molecules from approaching the active sites to undergo oxidation. This limitation is a major challenge today for Pd and platinum (Pt)-based electrocatalysts [10]. The stability and durability of these Pd-based electrocatalysts is another unsolved problem. For these reasons, the search for non-noble metals as co-catalysts has become the focus of several researchers.

These auxiliary metals would act by the bifunctional mechanism or electronic effect with the purpose of oxidizing the adsorbed intermediates in the surface of the catalytic metals and release the active site for the oxidation of a new molecule of the fuel [10–12]. Some binary electrocatalysts such as PdRu/C, PdIr/C, PdAu/C, PdSn/C and others have been proposed to improve the electrocatalytic activity, tolerance to impurities in the ethanol (and intermediate products from EOR), stability and durability of the materials [13–17]. Alvarenga and collaborators [12] showed that the EOR activity of Pd nanoparticles is strongly correlated with electronic properties and managed to use a lower onset potential in the EOR. Chen et al. [18] reported the use of PdRu/C for the oxidation reaction of bioethanol and evaluated the impurities' tolerance.

The most important properties for the catalyst are nanoparticle stability, durability and capability for the oxidation of CO to CO_2 [19]. Therefore, in order to proceed with the use of bioethanol as a fuel in FCs, we need to improve the tolerance of Pd to impurities/poisoning with the aid of an auxiliary metal. It has been shown that there is no low-cost auxiliary metal that exhibits all the desired effects (such as high stability and CO-tolerance). Nevertheless, there have been reports of auxiliary metals that obtain some desired effects, for example, Ru enhanced the surface area [20]; Sn improved the CO-tolerance by an electronic effect [21]; and other noble metals, e.g., Ag, Au, and Rh, or non-noble metals such as Fe,

Co, Ni, Cu and Mn have also been shown to improve the catalytic activity [22–31].

In this work, we present the synthesis of Pd and Nb electrocatalysts supported on carbon Vulcan XC72 by a simple and fast sol-gel method. We characterized the fabricated electrocatalysts by SEM/EDX, ICP-MS, TEM, XRD, and contact angle measurement techniques. The electrochemical activity, stability and mechanism were evaluated, and finally, the electrocatalysts were applied in the DEFC experiments.

Materials and methods

Preparation of the electrocatalysts

The electrocatalysts were prepared by a modified sol-gel method [32]. First, 57.8 mg (125 μmol) of Pd-acetylacetonate (99% Sigma-Aldrich®, product by USA) and 58.7 (215 μmol) mg of $NbCl_5$ (99% Sigma Aldrich® product by Germany) were mixed with 6 mL of isopropyl alcohol (Synth®) and 2 mL of acetic acid (Synth®). Then, 160 mg of Vulcan XC72 carbon was added. The sol-gel solution was homogenized by magnetic stirring and heated for 60 min to dryness. The samples were submitted to heat treatment in the muffle under N_2 atmosphere. The samples were heated at the rate of 5 °C min^{-1} in three steps: for the Pd_1Nb_1/C sample, at 110 °C for 15 min, at 400 °C for 60 min and then cooled at the rate of 10 °C min^{-1} until the sample reached room temperature. For other electrocatalysts, the same procedure was followed but with changes in the quantities of reagents, which were 115.6, 28.9 and 86.7 mg for Pd-acetylacetonate and 0, 88.1 and 29.3 mg for Niobium(V) chloride for these electrocatalysts Pd/C, Pd_1Nb_3/C and Pd_3Nb_1/C, respectively.

Electrochemical measurements

Electrochemical cell
The materials were electrochemically characterized, and their catalytic activity was evaluated by cyclic voltammetry (CV) and chronoamperometry (CA) using an Autolab 302N potentiostat. The electrolyte was KOH (1.0 mol L^{-1}) with or without ethanol (1.0 mol L^{-1}). A conventional electrochemical cell with a three-electrode configuration was used and included a 1.0 cm^2 platinum electrode as the counter electrode, Hg/Hg_2Cl_2 (SCE) as the reference electrode and the investigated electrocatalyst supported on a glassy carbon electrode as the working electrode.

The three electrodes were arranged in a 40 mL cell that contained the N_2-degassed (to reduce the O_2 intervention) electrolyte solution. For the analysis in the presence of ethanol, 2.34 mL of ethanol (99.5% Dinâmica®, Brazil) was added into the working solution to obtain a concentration of 1.0 mol L^{-1} for both the CV and CA tests. All experiments were carried out at room temperature.

Preparation of the working electrode
For the preparation of the electrocatalyst, we used approximately 8 mg of the metal/carbon mixture. Next, we added 1 mL of high purity deionized water (resistivity 18.2 MΩ cm, Millipore water purification system, Millipore, Bedford, MA,

USA) and sonicated this mixture for 40 min. Following homogenization, 20 μL of Nafion® solution (5% m/v) was added, and the mixture was sonicated for 30 min, generating a black and homogeneous dispersion. Finally, 20 μL of this dispersion was added onto the working electrode (glassy carbon) and dried using a tungsten lamp.

Physical characterization

X-ray diffraction (XRD) analysis
All electrocatalysts were physically characterized by X-ray diffraction (XRD). XRD was performed using a Rigaku-MiniFlex X-ray diffractometer with CuKα (λ = 1.54056 Å) radiation source operating continuously ($2°$ min^{-1}) from 20 to 80° (2θ) in order to determine the crystalline phases and to estimate the mean crystallite sizes.

Elemental composition by ICP-MS analysis
The elemental composition of the electrocatalysts was determined using an inductively coupled plasma mass spectrometer (ICP-MS, Agilent 7900, Hachioji, Japan) operated with high-purity argon (99.9999%, White Martins, Brazil). All reagents were of analytical grade. Nitric acid and HCl were purified by using a Teflon sub-boiling distiller (DST-100, Savillex, USA). High-purity deionized water (resistivity 18.2 MΩ cm) was generated with a Milli-Q water purification system (Millipore, Bedford, MA, USA). The extraction of Pd and Nb was carried out using a closed vessel system. Approximately 30 mg of electrocatalyst was placed into 100 mL test tubes that contained 3 mL of HNO$_3$ + 1 mL of HCl, and the test tubes were then closed. Then, the test tubes were stored for 24 h at 25 °C. After this step, the tubes were heated at 200 °C for 2 h in a graphite-covered digester block (EasyDigest, Analab, France). Finally, the volume was increased to 50 mL, and the elemental composition was determined by ICP-MS. The ^{105}Pd and ^{93}Nb isotopes were monitored. The limits of detection were 0.004 μg L^{-1} and 1.93 μg L^{-1} for Pd and Nb, respectively. During the analysis, we used ^{89}Y (25 μg L^{-1}) as the internal standard, and the calibration curve was obtained in the 1–50 μg L^{-1} range for Pd and Nb (R^2 = 0.9999).

Transmission electron microscopy (TEM)
To observe the morphology and to measure the particle sizes, transmission electron microscopy (TEM) analyses were performed using a high-resolution JEOL JEM-2100 electron transmission microscope operating at 200 kV. The samples for the TEM studies were prepared by placing nanodispersion droplets on a carbon-coated copper grid, followed by the evaporation of the solvent (water) at room temperature. The average particle sizes were measured using the ImageJ software package (v.1.50i; product of Wayne Rasband, National Institutes of Health, USA), and more than 300 different particles were analyzed.

Contact angle analysis
The contact angle measurements of Vulcan XC-72, Pd/C, Nb/C and the PdxNbx/C-based electrocatalysts were performed using a goniometer (GBXTM digidrop) to characterize the hydrophilicity of each material. Solutions of all materials with the concentration of 3 mg mL^{-1} (material/chloroform) were

prepared and were sonicated for 60 min in an ultrasonic bath. Then, 60 μL aliquots of each dispersion were deposited on a glassy carbon (GC) plate and dried in order to form a thin and homogeneous film on the GC substrate. Thereafter, 5 μL of distilled water was dropped on the formed film to determine the contact angles. The contact angle measurements were performed at the time of the drop placement and every minute after, for 5 min. The measurements were performed in triplicate using the Windrop ++ software.

Analysis of ATR-FTIR ex situ
The ATR-FTIR measurements were performed using a Varian® 660 IR spectrometer equipped with an MCT detector cooled by liquid N$_2$ and an ATR accessory (MIRacle with a Diamond/ZnSe Crystal Plate Pike®). The spectra were computed from 128 interferograms averaged from 4000 cm^{-1} to 850 cm^{-1} with the spectral resolution set to 8 cm^{-1}. Aliquots of 20 mL of the products (residual liquids after the reactions in the fuel cell) generated during the 30 min of the fuel cell operation were taken from the oxidized fuel (Ethanol + KOH solution) in the DEFC. Then, these residues were stored in a refrigerator at the temperature of 10 °C for 3–5 days from the day of the FTIR ex situ analysis.

Direct ethanol fuel cell (DEFC) experiment

Treatment of Nafion
Nafion membranes (N117, DuPont®) underwent the standard procedure for cleaning and anionic activation with successive washing steps. The first step consisted of immersing the membranes in H$_2$SO$_4$ (1 mol L^{-1}) and H$_2$O$_2$ (3 vol%) solutions at 80 °C for 1 h, respectively, between immersing in solution above the membranes and washing once with deionized water (resistivity 18.2 MΩ cm, Millipore). The second step consisted of immersing the membranes in the KOH solution (6 mol L^{-1}) for 24 h and then subjecting the membranes to three washings with deionized water (resistivity 18.2 MΩ cm, Millipore) at 80 °C for 1 h. Then, the Nafion® membranes were stored in 6 mol L^{-1} of KOH solution until the time that they were washed and could be used in fuel cells experiments.

MEA preparation
For the membrane electrode assemblies (MEAs), the anode and cathode were prepared using the synthesized catalysts and Nafion® 5% solution loadings of 1.0 mg cm^{-2} and 30 wt%, respectively. The MEAs were prepared by hot-pressing a pre-treated Nafion® 117 membrane placed between a BASF commercial cathode (1 mg$_{(Pt)}$ cm^{-2}) and a homemade anode (1 mg$_{(Pd)}$ cm^{-2}) at 130 °C for 420 s, under the pressure of 225 kgf cm^{-2}. The MEA was placed between two bipolar plates and assembled in a single fuel cell with a 3 Nm torque wrench.

DEFC experiment
The fuel cell operating performance characteristics were determined in a monoplanar DEFC with the geometric surface area of the electrodes of 5.0 cm^2 using a test bench obtained from the Electrocell Group that allows the control over the fuel cell operating parameters (flow rates, humidification and temperature of the reactants and cell) and performs automatic data acquisition of polarization curves and power

density curves in real time. Liquid fuel alimentation was carried out with the use of a Masterflex L/S Cole-Parmer peristaltic pump. The temperature was set between 50 and 90 °C for the fuel cell and to 85 °C for the oxygen humidifier. The fuel of 2.0 mol L^{-1} of ethanol (1.0 mol L^{-1} of KOH) was delivered at the rate of 1.0 mL min^{-1}, and the oxygen flow was set to 200 mL min^{-1}. The single fuel cell was stabilized for 90 min at the constant measurement temperature. Polarization curves were collected using a potentiostat/galvanostat Autolab PGSTAT 302N.

Results and discussion

Physico-chemical characterizations and electrochemical activity studies

The physico-chemical characterizations were conducted previously and are described in a recent report by our group [33].

Briefly, the nominal mass concentrations of Pd were 20, 15, 10 and 5%, and the mass ratios obtained by ICP-MS of Pd were 26.5 ± 2.6, 13.7 ± 0.7, 8.8 ± 0.6 and 4.3 ± 0.1% for Pd/C, Pd$_3$Nb$_1$/C, Pd$_1$Nb$_1$/C and Pd$_1$Nb$_3$/C electrocatalysts, respectively. The nominal mass concentrations of Nb were 5, 10 and 15%, and the mass fractions of Nb obtained by ICP-MS were 4.55 ± 0.7, 13.4 ± 3.6 and 13.6 ± 1.9% for Pd$_3$Nb$_1$/C, Pd$_1$Nb$_1$/C and Pd$_1$Nb$_3$/C electrocatalysts, respectively. The real Pd to Nb atomic ratios were 70:30, 40:60 and 22:78 for Pd$_3$Nb$_1$/C, Pd$_1$Nb$_1$/C and Pd$_1$Nb$_3$/C electrocatalysts, respectively. The Pd mass concentration values obtained by ICP-MS were used to normalize the results of the electrochemical studies in which Pd$_1$Nb$_1$/C was found to show the highest enhancement of the electrocatalytical activity for EOR.

Souza et al. [33] have shown that the electrochemical active surface areas (ECSA) of the electrocatalysts can be estimated by electrochemical oxidation of a pre-adsorbed saturated CO adlayer. The order of ECSA values obtained by CO-stripping is Pd$_3$Nb$_1$/C < Pd/C < Pd$_1$Nb$_1$/C < Pd$_1$Nb$_3$/C, with 13, 29, 10 and 47 m^2 g^{-1} of Pd, respectively. The Pd$_1$Nb$_1$/C electrocatalyst showed the lowest onset potential (−0.54 V) for CO oxidation that was more negative than those of the commercial Pd/C (−0.50 V), Pd$_3$Nb$_1$/C (−0.38 V) and Pd$_1$Nb$_3$/C (−0.35 V) catalysts. These results were reported and indicated the existence of a bifunctional mechanism and the lowest poisoning by the strongly bound CO.

Previous work has shown that the Pd$_1$Nb$_1$/C electrocatalyst exhibits the lowest onset potential of ~−0.30 V vs. RHE compared to the other electrocatalysts reported previously. Therefore, DEFC applications (ΔE$_{cell}$ = E$_c$ - E$_a$ = ~0.85 − (−0.30)) are operated at ~1.15 V (considering that a fuel cell cathode typically operates at ~0.85 V RHE). Therefore, we will further evaluate and validate these values in DEFC experiments in this work because of the great potential for DEFCs in the alkaline medium.

The results of the XRD analysis showed that the electrocatalysts are a mixture of metals and oxides of Pd and Nb. No shift of the metallic Pd or Nb peaks was observed because the network parameter derived from XRD results was 0.388 nm for all electrocatalysts studied. This suggests that there is no

alloying of the Pd with the Nb. Therefore, the electronic effect should not be dominant, while the bifunctional effect could be dominant for the EOR [34]. The presence of Nb slightly increases the mean crystallite size of the Pd nanoparticles according to the Debye-Scherrer formula [33] because the average crystallite sizes were 4.0 ± 1.6, 4.1 ± 1.1, 4.6 ± 1.3 and 4.7 ± 1.0 nm for the Pd/C, Pd$_1$Nb$_1$/C, Pd$_3$Nb$_1$/C and Pd$_1$Nb$_3$/C electrocatalysts, respectively.

TEM images showed a random distribution of the nanoparticles on the Vulcan XC72 carbon support with the average particle diameters of 9.1 ± 3.4, 6.4 ± 3.0, 3.4 ± 1.2 and 12.5 ± 4.5 nm, respectively, for Pd/C, Pd$_1$Nb$_1$/C, Pd$_3$Nb$_1$/C and Pd$_1$Nb$_3$/C. It can be seen in Fig. 1 that Pd nanoparticles are spherically shaped, and for both metals, the nanoparticles are found in some clusters, and the spherically shaped nanoparticles are totally dispersed.
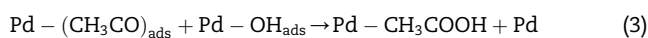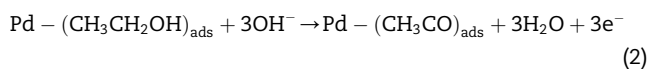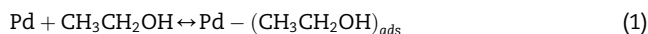
The Pd$_3$Nb$_1$/C and Pd$_1$Nb$_1$/C electrocatalysts showed the smallest nanoparticle average diameter. These results indicate that these electrocatalysts had a higher surface area per mass of catalytic metal.

Electrocatalyst property studies

Contact angle results
Although the hydrophilicity of the electrocatalysts is important to the management of the reagents and product diffusion in DEFC, it plays a significant role in the EOR of the electrocatalysts for the alkaline medium, as discussed below.

Based on a previous study [35], the mechanism of EOR on Pd in an alkaline medium can be described by the following Reactions (1)−(4):

$$Pd + CH_3CH_2OH \leftrightarrow Pd - (CH_3CH_2OH)_{ads} \quad (1)$$

$$Pd - (CH_3CH_2OH)_{ads} + 3OH^- \rightarrow Pd - (CH_3CO)_{ads} + 3H_2O + 3e^- \quad (2)$$

$$Pd - (CH_3CO)_{ads} + Pd - OH_{ads} \rightarrow Pd - CH_3COOH + Pd \quad (3)$$

$$Pd - CH_3COOH + OH^- \rightarrow Pd + CH_3COO^- + H_2O \quad (4)$$

Reactions (1) and (2) are generally accepted to occur at the potential region less than −0.7 V vs. SCE in the anodic sweep. The CH$_3$CO$_{ads}$ or other carbonaceous reactive intermediates will strongly absorb on the surface of Pd and block the active sites. Reactions (3) and (4) occur in the region higher than −0.7 V vs. SCE, where Pd begins to adsorb OH$^-$. With the adsorption of hydroxyl on Pd or Nb, the strongly absorbed carbonaceous species will be quickly stripped away and result in the increase of the current. However, to preserve the adsorption of OH$^-$ on the Pd, it is necessary that the water molecules adsorb on Pd and then dissociate, as described by Reaction (5) [36].

$$H_2O_{ads}(weakly\ adsorbed) \rightarrow OH_{ads} + H^+ + e^- \quad (5)$$
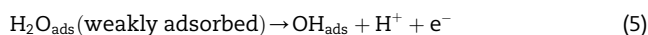
Thus, the dissociation Reaction (5) on the surface near the active sites of the Pd should be favored for the continuity of the ethanol dehydrogenation reaction, Reaction (3). However, it is likely that the water adsorption and dissociation are governed by the potential at which Reaction (5) occurs, and in
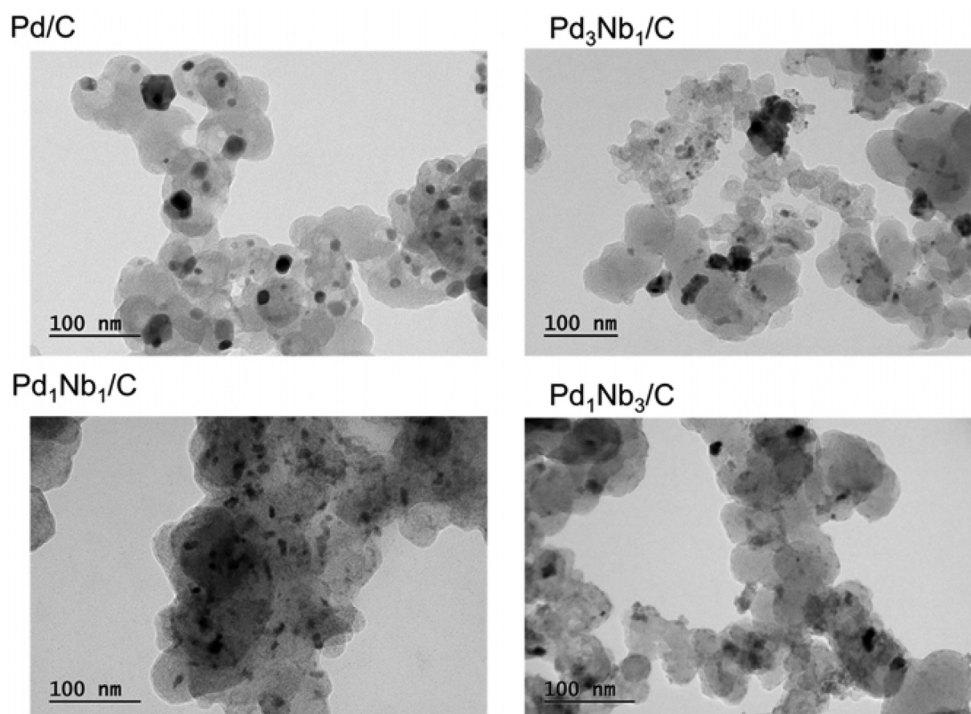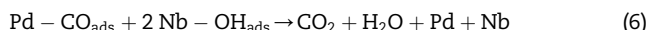
Fig. 1 – TEM electrocatalyst images.

this case, Pd and Nb oxides can contribute by oxidizing the strongly bound intermediates such as CO because CO stripping is followed by the reaction between the formed Pd or Nb-OH_{ads} and Pd-CO_{ads}, Reaction (6):

$$Pd - CO_{ads} + 2\,Nb - OH_{ads} \rightarrow CO_2 + H_2O + Pd + Nb \qquad (6)$$

because Reaction 5 can occur at the low potentials for Pd_xNb_y electrocatalysts [37,38].

Through the analysis of the contact angle, we can understand how the hydrophilicity of the materials was modified compared to the Vulcan XC72 precursor material. Table 1 shows the contact angle of the materials that is related to the hydrophilicity of the electrocatalysts.

According to Table 1, all synthesized electrocatalysts became more hydrophobic after the synthesis. We noticed that Nb is more hydrophobic than Pd, but this did not govern the properties of the electrocatalyst after the sol-gel synthesis. In general, no relevant differences in the hydrophilicities of all of the Pd_xNb_y/C electrocatalysts were found to justify the different electrocatalytical activities of the studied electrocatalysts. This suggests that water does not have a major influence on the EOR catalysis, in accordance with Reactions 3–5.

Kinetic study for EOR

The kinetic study for EOR allowed us to explain the role of Nb. We performed an LSV at the sweep rate of 1 mV s^{-1} experiment near a pseudo steady-state within the range of the potential, 0.50 to −0.32 V vs. SCE. From the EOR curves obtained in this experiment, it was possible to obtain the Tafel slope, as defined by the mathematical relation of Eq. (6)

$$\eta = -\frac{2.303\,RT}{\beta F}\log i_0 + \frac{2.303\,RT}{\beta F}\log i \qquad (6)$$

where η is the overpotential, β is the anodic transfer coefficient or symmetry, i_0 is the exchange current density, i is the current density, R is the universal gas constant, F is the Faraday constant and T is the temperature [39]. This equation shows the linear relationship between the overpotential and the current density logarithm, which is displayed in Fig. 1. The slope of the line in Fig. 2 is the Tafel slope, which is equal to 2.303RT/βF, and the obtained Tafel slope was derived in the low potential range from −0.50 to −0.32 V vs. SCE by plotting the overpotential, η, versus the logarithm of the current density. The exchange current density (i_0) was obtained by extrapolating the fitted Tafel line to where the overpotential equals zero, and from the linear coefficient of the curve, it is possible to obtain β.

We can observe that only the Pd/C electrocatalyst has the EOR governed by two determining steps because it shows two

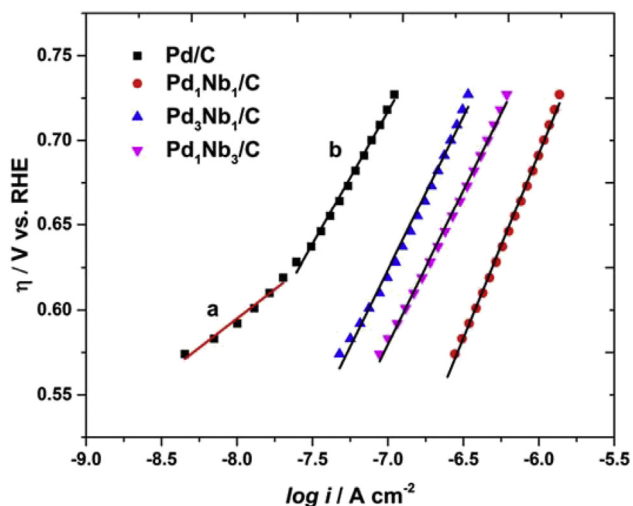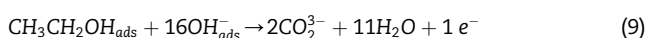| Table 1 – Average contact angles of the electrocatalysts.	
Electrocatalyst	Contact angle
C (Vulcan XC72)	66 ± 4
Nb/C	94 ± 2
Pd/C	76 ± 3
Pd$_1$Nb$_1$/C	76 ± 2
Pd$_1$Nb$_3$/C	72 ± 1
Pd$_3$Nb$_1$/C	71 ± 1

Fig. 2 – Tafel plot of EOR from LSV using 1.0 mol L^{-1} of ethanol and 1.0 mol L^{-1} of KOH, measured over potential range from −0.50 to −0.32 V vs. SCE at temperature room. The potentials measured versus SCE were rescaled to the reversible hydrogen electrode (RHE) scale according to the Nernst equation: $E_{RHE} = E_{SCE}+0.242 + 0.059$ pH.

straight lines between 570 mV and 730 mV, i.e., two different slopes (a and b in Fig. 2). Unlike for the other electrocatalysts that contain Nb, here, the EOR occurs by a single determining step due to the presence of only one slope in Fig. 2. The EOR is complex and may result in several final byproducts, including an undesirable acetaldehyde (CH_3CHO) and acetic acid (CH_3COOH) or acetate (CH_3COO^-) products, described by Reactions (7) and (8), respectively. Carbon dioxide (CO_2) is the desirable product, obtained as described by Reaction (9) [40].

$$CH_3CH_2OH_{ads} + 2OH^-_{ads} \rightarrow CH_3CHO_{ads} + 2H_2O_{ads} + 2e^- \qquad (7)$$

$$CH_3CH_2OH_{ads} + 5OH^-_{ads} \rightarrow CH_3CHO^-_{ads} + 4H_2O_{ads} + 4e^- \qquad (8)$$

$$CH_3CH_2OH_{ads} + 16OH^-_{ads} \rightarrow 2CO_2^{3-} + 11H_2O + 1\,e^- \qquad (9)$$

Each of these reactions has different pathways and at least one rate determining step. In actual reaction conditions, the pathways (7), (8) and (9) compete with each other. Hence, the presence of Nb may have changed the reaction mechanism for EOR, avoiding some unnecessary reaction steps and making EOR proceed by a pathway with only a single rate-determining electrochemical step [40]. Based on the high Tafel slopes (e.g. 217 mV dec^{-1}) in electrocatalysts for EOR, the results indicated that kinetics are too complex according to the results of references [39,41], which found the Tafel slope values in the 200−500 mV dec^{-1} range at low and high potentials, respectively. This indicates that the whole process is not only controlled by the adsorbed OH$^-$ ions (Reaction (5)) but also affected by the surface reactions as oxides in addition to the hydroxyl ion adsorption. The alloying with Nb most likely does not only modify the intrinsic activity of Pd but also exposes more active sites. If the number of exposed sites of palladium in the presence of

niobium oxides is enhanced, we can expect a low poisoning by adsorbed CO, as we can see on page 12, as previously reported [33] and in Reaction (6) above. Another important point is that in the presence of niobium oxides, the OH species that could be formed on Pd are formed at low potentials, liberating the Pd sites for EOR.

The results summarized in Table 2 show the exchange current density toward EOR on Pd/C and Pd$_x$Nb$_y$/C electrocatalysts. We note that the highest current exchange densities are obtained using the electrocatalysts with Nb. The highest exchange current density is achieved on Pd$_1$Nb$_1$/C obtaining 6.6×10^{-10} A cm^{-2}, which is 244 times larger than the current density for Pd/C (2.7×10^{-12} A cm^{-2}). This showed that Nb increased the electron exchange rate at the analyte/electrode interface, enhancing the kinetics of the EOR reaction [42].

The anodic transfer coefficient (β) is a measure of the symmetry of the activation barrier and varies from 0 to 1 for both the direct and inverse reactions. In the case of the EOR, the β value closer to zero has a smaller activation barrier for the continuation of the reaction in the determinant slow step

Table 2 – Tafel slope, anodic transfer coefficient and exchange current density results.

Electrocatalysts	Tafel slope (mV dec^{-1})	β − anodic transfer coefficient	i_0 (A cm^{-2})
Pd/C[a]	68.8	0.85	2.3×10^{-17}
Pd/C[b]	156.8	0.37	2.7×10^{-12}
Pd$_1$Nb$_1$/C	217.4	0.27	6.6×10^{-10}
Pd$_3$Nb$_1$/C	180.9	0.32	3.6×10^{-11}
Pd$_1$Nb$_3$/C	184.8	0.32	7.3×10^{-11}

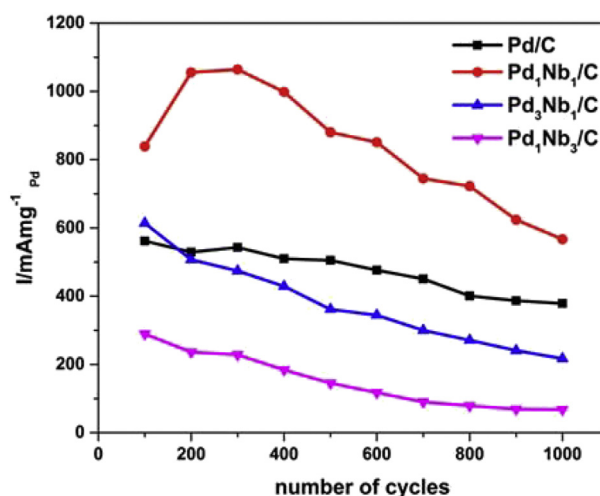[a] Refers to the first (red line) and [b] the second (line black) slope of the Tafel curve of Pd/C in Fig. 2.

Fig. 3 – Peak current density for EOR using Pd$_x$Nb$_y$/C electrocatalysts in the accelerated durability test during 1000 voltammetric cycles using 1.0 mol L^{-1} of ethanol and 1.0 mol L^{-1} of KOH, measured over the potential range from −0.80 to +0.20 V vs. SCE, at the scan rate of 100 mV s^{-1} at room temperature.

[42]. From the data presented in Table 2, we can see that Pd_1Nb_1/C has the lowest β (close to zero), suggesting that Pd_1Nb_1/C has a smaller activation barrier, providing additional support for the conclusion that the best electrocatalytic activity is displayed by Pd_1Nb_1/C [21].

Accelerated durability test (ADT) experiment with ICP-MS analysis

The stability of the nanoparticles and the durability of the catalytic activity of the electrocatalysts is another challenge
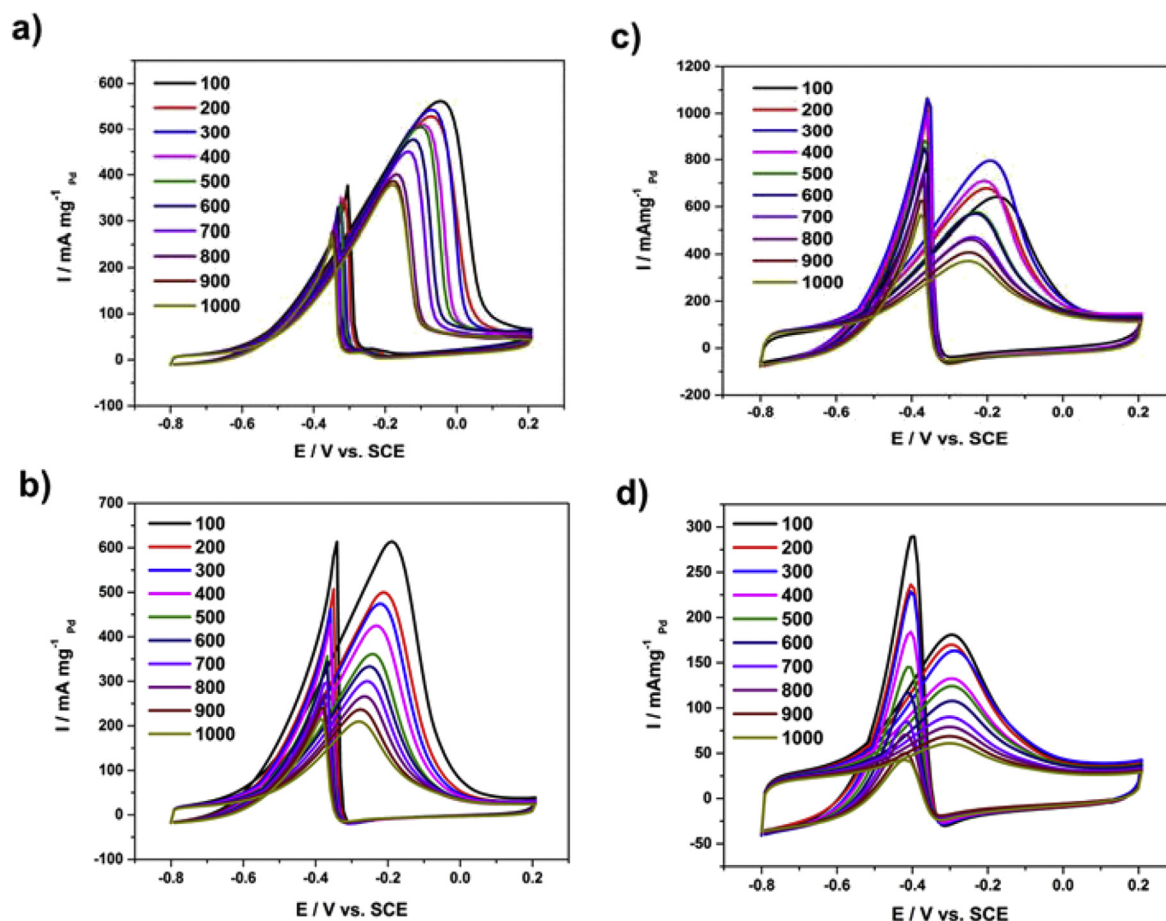

Fig. 4 — Cyclic voltammograms for EOR using the electrocatalysts a) Pd/C, b) Pd_3Nb_1/C, c) Pd_1Nb_1/C and d) Pd_1Nb_3/C with 1.0 mol L^{-1} of ethanol and 1.0 mol L^{-1} of KOH, measured over the potential range from −0.80 to +0.20 V vs. SCE, at the sweep rate of 100 mV s^{-1} at room temperature.
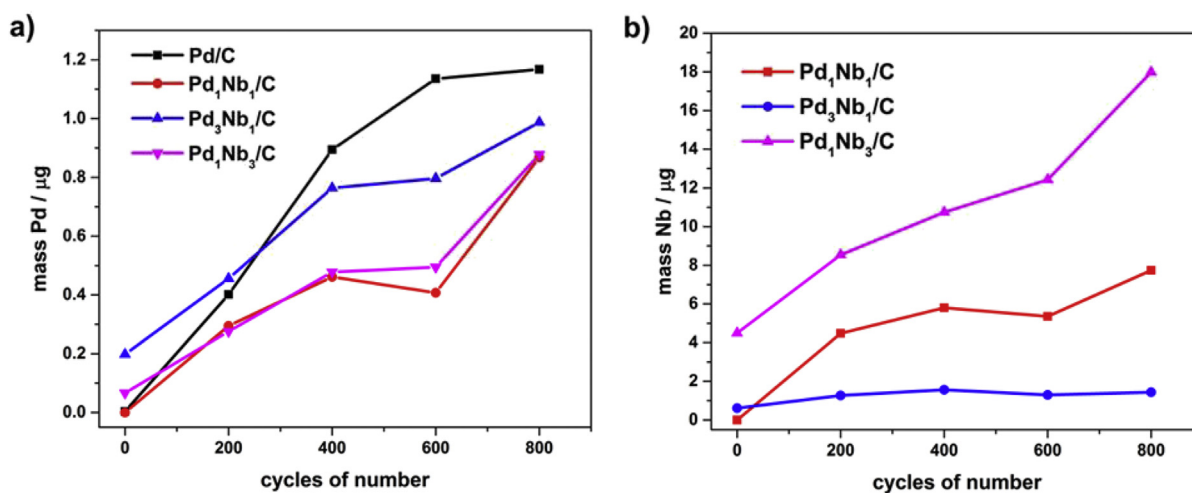

Fig. 5 — Metal mass of a) Pd and b) Nb worn out from the electrocatalysts during the accelerated durability test. All electrocatalysts have equal Pd amounts at the beginning of the experiment.

that must be overcome for the application of DEFC technology. To evaluate the durability of the Pd_xNb_y/C electrocatalysts, ADT was performed by 1000 voltammetric cycles of EOR, monitoring the dissolution of the Pd and Nb metals from the electrocatalysts, after each 200 cycles by ICP-MS analysis. All electrocatalysts showed some stability at the peak current density for EOR. However, Pd_1Nb_1/C showed the highest peak current density as well as the greatest stability along the ADT, as shown in Figs. 3 and 4.

From Fig. 5 we observe the metal dissolution from the electrocatalysts to the electrolyte due to the electrochemical stress conditioned by the ADT experiment. The Pd_1Nb_1/C electrocatalyst shows the lowest dissolution of the Pd metal into the solution, justifying its higher peak current densities shown in Fig. 5a. Meanwhile, Pd_3Nb_1/C had the lowest dissolution of Nb, as expected, because it has the lowest amount of Nb in the electrocatalysts, as shown in Fig. 5b.

Pd_1Nb_1/C electrocatalysts had the lowest Pd mass loss after the ADT of 1.49% compared to the initial mass of the experiment and lower loss of mass of Nb than Pd_3Nb_1/C, although Pd_3Nb_1/C had a lower amount of Nb at the start of the experiment, according to Table 3.

These results indicated that Pd_1Nb_1/C has high electrochemical activity and good durability for EOR, showing it to be a promising electrocatalyst for application in DEFCs.

Direct ethanol fuel cell (DEFC) experiment

The performance of the Pd_xNb_y/C electrocatalysts was evaluated in a monoplanar DEFC. First, the ideal working temperature was evaluated using the commercial reference material Pd/C, as shown in Fig. 6a. We can see that the best performance for the Pd/C electrocatalyst was obtained at 50 °C. Using this information, we performed the test for all electrocatalysts at this same temperature, following Fig. 6b. All electrocatalysts with different proportions of Niobium showed better performance than Pd/C. The Pd_1Nb_1/C electrocatalyst achieved the best catalytic performance, which was 1.80 times higher than that of Pd/C (with power densities of 13.53 and 7.50 mW cm^{-2}, respectively). In other words, Nb improved the catalytic activity of Pd for EOR in the alkaline medium, supporting the previous electrochemical results. Finally, the experiments to optimize the working temperature for the Pd_1Nb_1/C electrocatalyst were performed. According to

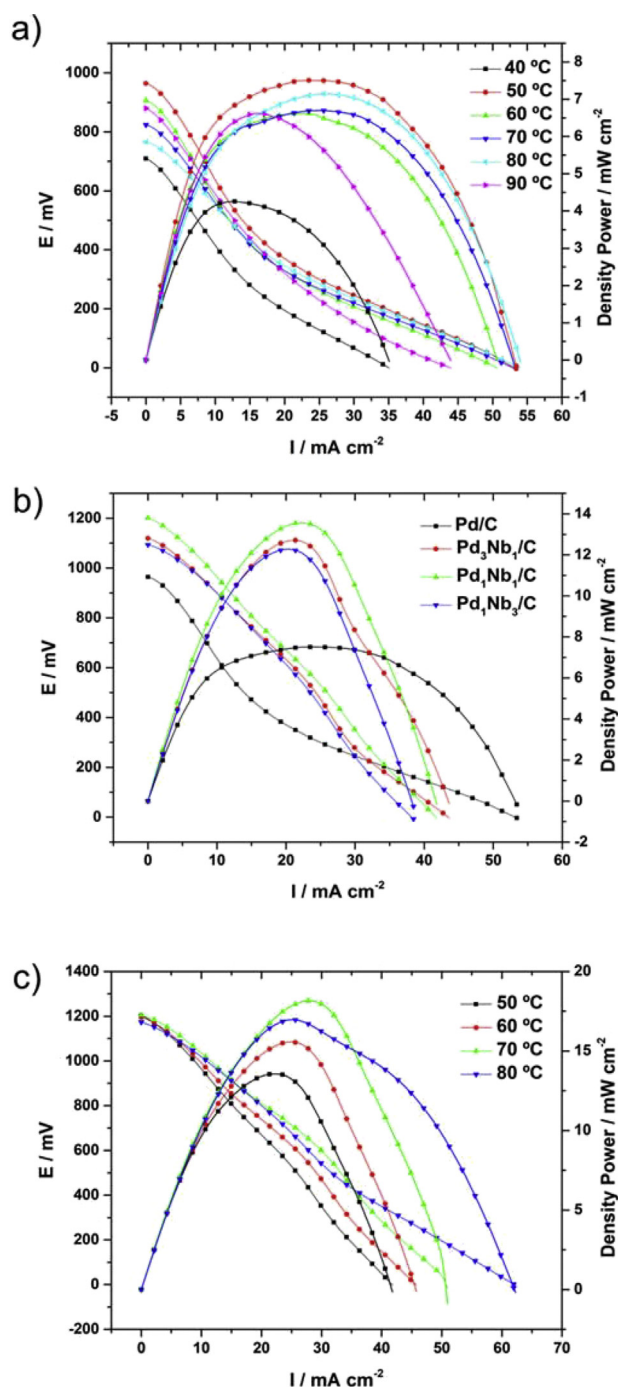Fig. 6 — Polarization and power density curves in DEFC a) Pd/C in different temperatures, b) Pd/C and Pd_xNb_yC electrocatalysts at 50 °C and c) Pd_1Nb_1/C in different temperatures.

Fig. 6c, the best performance was obtained at 70 °C for $Pd_1Nb_1/$ C, reaching 18.11 mW cm^{-2}. We suggest that the obtained results mainly originate from the bifunctional effect due to niobium oxide [43].

While some results for the alkaline DEFC have been reported in the literature, the comparison of our results with these studies is very difficult due the different materials (anionic membranes and catalysts) and conditions used

Table 3 — Results of Pd and Nb metal loss after accelerated durability.

Electrocatalyst	Loss of Pd after ADT (%)	Loss of Nb after ADT (%)
Pd/C	5.41 ± 0.09	n.d.
Pd_1Nb_1/C	1.49 ± 0.03	14.40 ± 0.39
Pd_3Nb_1/C	4.02 ± 0.11	15.09 ± 0.22
Pd_1Nb_3/C	7.82 ± 0.81	37.13 ± 0.76

Obs.: Amount in weight percentage of metal loss compared to the initial metal mass in the catalytic layer on the surface of the glassy carbon electrode. All electrocatalysts' initial masses were determined by ICP-MS.

(quantity of catalysts on anodes and cathodes, temperature, etc.). For comparison, we can use the PdSn alloy in the 90:10 ratio that was reported by Da Silva [44], which achieved the maximum power density of 15 mW cm^{-2} under the conditions similar to those of our work, compared to the power density of 18 mW cm^{-2} at the 50:50 ratio achieved in this work. PdSn alloys have been the most developed materials for alkaline DEFCs recently.

FTIR experiment

ATR-FTIR experiments were performed to correlate the activity of ethanol electrooxidation with a preferential mechanism. The FTIR spectra in the region between 2500 and 850 cm^{-1} were recorded after the collection of the products from a single DEFC in the alkaline media, using 1 mol L^{-1} of KOH and 2 mol L^{-1} of CH$_3$CH$_2$OH for all electrocatalysts, as shown in Fig. 7. From the ATR-FTIR results, it was possible to observe the appearance of bands at 2343 cm^{-1} related to the CO$_2$ formation [45]. The acetate was displayed as two intense peaks at 1553 and 1410 cm^{-1}, arising from asymmetric and symmetric C—O bond vibrations [46]. A carbonate ion band at 1370 cm^{-1} was not clearly visible in the spectra, due to the

overlap with the acetate band at 1410 cm^{-1}, even though its presence can be inferred by the deconvolution of the spectra, as reported by Neto et al. [47]. Even though the peak at 926 cm^{-1} is associated with the acetaldehyde C—C—O stretching vibrations, the appearance of this peak was not pronounced in the electrocatalysts, except for Pd/C. This suggests that the addition of Nb to Pd-based electrocatalysts showed a single rate-determining step for EOR as indicated by the Tafel analysis results in this work. In the spectra, it is also possible to observe the presence of bands of ethanol that were not consumed during the DEFC experiment (1080 cm^{-1}, 1036 cm^{-1} and 874 cm^{-1}) [45].

Fig. 8a shows an FTIR spectrum in a large spectral window in which we can see qualitatively that Pd$_1$Nb$_1$/C has the largest band for CO$_2$ formation after a single DEFC test. This can be seen more clearly after all bands were deconvoluted to Lorentzian line forms [47] of the CO$_2$ and acetate. Then, we integrated the intensities of the bands specific to these chemical species, as shown in Fig. 8b, c and d.

We note that the most active electrocatalysts (Pd$_1$Nb$_1$/C) in the EOR experiments show an increase in the signal intensity of CO$_2$ production despite the higher formation of both acetate and CO$_3^{2-}$.
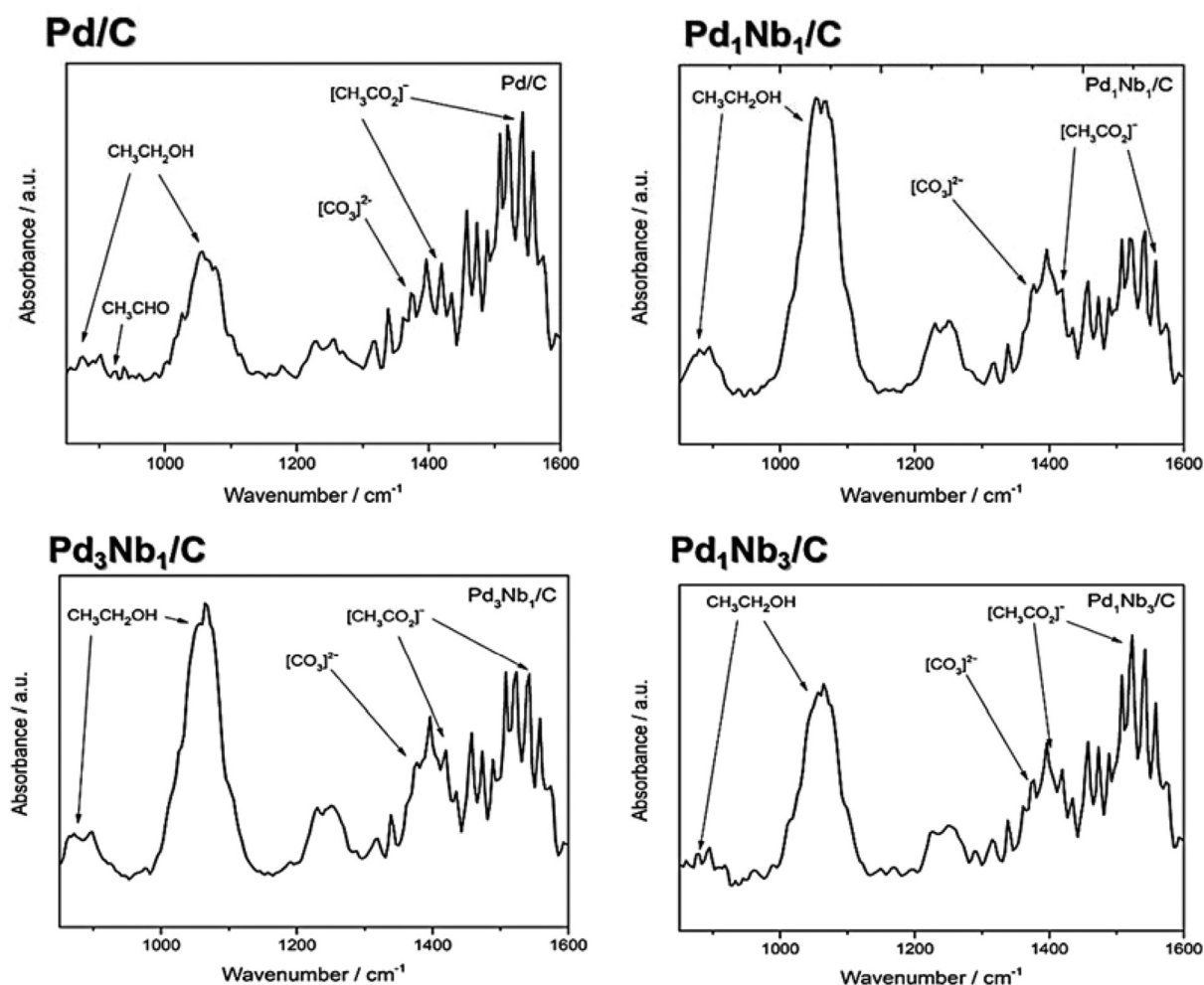

Fig. 7 — ATR-FTIR spectra collected from the products of the single DEFC in the alkaline medium, using 1 mol L^{-1} of KOH and 2 mol L^{-1} of CH$_3$CH$_2$OH of the prepared electrocatalysts. Aliquots from the experiment of Fig. 6b.
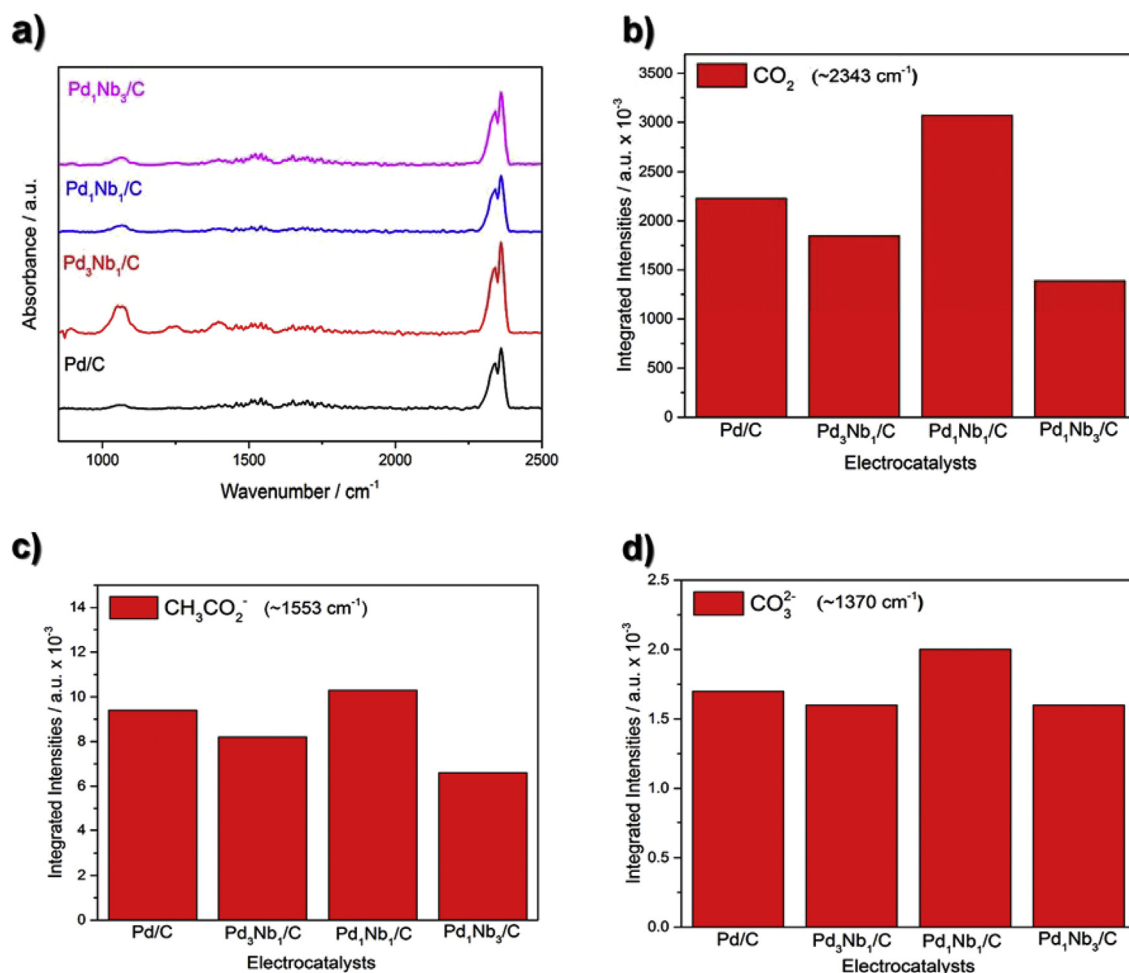
Fig. 8 – a) ATR-FTIR spectra in an expanded region and normalized intensity of b) CO_2, c) acetate and d) CO_3^{2-} bands for the electrocatalysts. Data are extracted from Fig. 7.

In summary, the experiments showed that the Pd_1Nb_1/C electrocatalyst exhibits promising activity for EOR, and the FTIR results strengthened the evidence that the presence of Nb modified the mechanism for EOR on Pd electrocatalysis to a mechanism that shows almost no formation of acetaldehyde, avoiding Reaction (7) [48]. Bianchini et al. [49] showed that the oxidative C−C bond cleavage of ethanol on Pd can occur when pH is in the 12−13 range, and metal oxides would increase the concentration of OH_{ads} species on the catalyst surface, favoring the reaction of the acetaldehyde into the carboxylic acid via $acyl_{ads}$-OH_{ads} coupling [49]. In this case, the presence Nb_2O_5 in our Pd_xNb_y/C electrocatalysts probably conducts the reaction at the same pathway as that reported in Ref. [49].

which gave rise to the reduced formation of acetaldehyde, an undesirable intermediate product. All electrocatalysts with Nb showed higher current exchange density values for EOR than Pd/C. The best performance for DEFC was obtained using Pd_1Nb_1/C, achieving the power density of 18.11 mW cm^{-2}, which confirmed the previous results of activity for EOR. The FTIR spectra indicated that Pd_1Nb_1/C displayed the highest production of CO_2 and the lowest production of acetaldehyde. Furthermore, the ADT experiments with ICP-MS analysis showed that Pd_1Nb_1/C obtained the highest peak current density during 1000 cycles of the experiment, presenting the lowest Pd mass loss after the ADT. Therefore, Pd:Nb binary electrocatalysts are a very promising choice for electrocatalysts in DEFCs using the alkaline media.

Conclusions

The Pd_1Nb_1/C electrocatalyst with the Pd/Nb mass ratio of 50:50 showed superior activity for EOR compared to Pd/C, Pd_3Nb_1/C and Pd_1Nb_3/C. The use of Nb in the Pd-electrocatalyst provided selectivity for a single rate-determining step for EOR,

Acknowledgements

REFERENCES

[1] McNicol B, Rand DA, Williams K. Direct methanol–air fuel cells for road transportation. J Power Sources 1999;83:15–31. https://doi.org/10.1016/S0378-7753(99)00244-X.

[2] Yuan T, Yang J, Wang Y, Ding H, Li X, Liu L, et al. Anodic diffusion layer with graphene-carbon nanotubes composite material for passive direct methanol fuel cell. Electrochim Acta 2014;147:265–70. https://doi.org/10.1016/j.electacta.2014.09.124.

[3] Sieben JM, Duarte MME. Nanostructured Pt and Pt–Sn catalysts supported on oxidized carbon nanotubes for ethanol and ethylene glycol electro-oxidation. Int J Hydrogen Energy 2011;36:3313–21. https://doi.org/10.1016/j.ijhydene.2010.12.020.

[4] An L, Zhao TS, Shen SY, Wu QX, Chen R. Performance of a direct ethylene glycol fuel cell with an anion-exchange membrane. Int J Hydrogen Energy 2010;35:4329–35. https://doi.org/10.1016/j.ijhydene.2010.02.009.

[5] Bambagioni V, Bianchini C, Chen Y, Filippi J, Fornasiero P, Innocenti M, et al. Energy efficiency enhancement of ethanol electrooxidation on Pd-CeO$_2$/C in passive and active polymer electrolyte-membrane fuel cells. ChemSusChem 2012;5:1266–73. https://doi.org/10.1002/cssc.201100738.

[6] Pereira JP, Falcão DS, Oliveira VB, Pinto AMFR. Performance of a passive direct ethanol fuel cell. J Power Sources 2014;256:14–9. https://doi.org/10.1016/j.jpowsour.2013.12.036.

[7] Bambagioni V, Bianchini C, Marchionni A, Filippi J, Vizza F, Teddy J, et al. Pd and Pt–Ru anode electrocatalysts supported on multi-walled carbon nanotubes and their use in passive and active direct alcohol fuel cells with an anion-exchange membrane (alcohol=methanol, ethanol, glycerol). J Power Sources 2009;190:241–51. https://doi.org/10.1016/j.jpowsour.2009.01.044.

[8] Jiang L, Hsu A, Chu D, Chen R. Ethanol electro-oxidation on Pt/C and PtSn/C catalysts in alkaline and acid solutions. Int J Hydrogen Energy 2010;35:365–72. https://doi.org/10.1016/j.ijhydene.2009.10.058.

[9] Beyhan S, Uosaki K, Feliu JM, Herrero E. Electrochemical and in situ FTIR studies of ethanol adsorption and oxidation on gold single crystal electrodes in alkaline media. J Electroanal Chem 2013;707:89–94. https://doi.org/10.1016/j.jelechem.2013.08.034.

[10] Silva J, De Souza R, Romano M. PtSnIr/C anode electrocatalysts: promoting effect in direct ethanol fuel cells. J Braz 2012;23(6):1146–53. http://www.scielo.br/scielo.php?pid=S0103-50532012000600021&script=sci_arttext&tlng=pt. [Accessed 4 April 2017].

[11] Wang H, Wang C, Yan H, Yi H, Lu J. Precisely-controlled synthesis of Au@ Pd core–shell bimetallic catalyst via atomic layer deposition for selective oxidation of benzyl alcohol. J Catal 2015;324:59–68. http://www.sciencedirect.com/science/article/pii/S0021951715000299. [Accessed 4 April 2017].

[12] Alvarenga G, Gallo I, Villullas H. Enhancement of ethanol oxidation on Pd nanoparticles supported on carbon-antimony tin oxide hybrids unveils the relevance of electronic effects. J Catal 2017;348:1–8. http://www.sciencedirect.com/science/article/pii/S0021951717300362. [Accessed 4 April 2017].

[13] Silva J, Parreira L, De Souza R. PtSn/C alloyed and non-alloyed materials: differences in the ethanol electro-oxidation reaction pathways. Appl Catal B 2011;110:141–7. http://www.sciencedirect.com/science/article/pii/S0926337311004127. [Accessed 5 April 2017].

[14] Shen S, Zhao T, Xu J. Carbon-supported bimetallic PdIr catalysts for ethanol oxidation in alkaline media. Electrochim Acta 2010;55(28):9179–84. http://www.sciencedirect.com/science/article/pii/S0013468610011771. [Accessed 5 April 2017].

[15] Ramulifho T, Ozoemena K, Modibedi R, Jafta C. Fast microwave-assisted solvothermal synthesis of metal nanoparticles (Pd, Ni, Sn) supported on sulfonated MWCNTs: Pd-based bimetallic catalysts for ethanol. Electrochimica 2012;59:310–20. http://www.sciencedirect.com/science/article/pii/S0013468611016239. [Accessed 5 April 2017].

[16] Modibedi R, Masombuka T, Mathe M. Carbon supported Pd–Sn and Pd–Ru–Sn nanocatalysts for ethanol electro-oxidation in alkaline medium. Int J Hydrogen Energy 2011;36(8):4664–72. http://www.sciencedirect.com/science/article/pii/S0360319911000383. [Accessed 5 April 2017].

[17] Dutta A, Mahapatra S, Datta J. High performance PtPdAu nano-catalyst for ethanol oxidation in alkaline media for fuel cell applications. Int J Hydrogen Energy 2011;36(22):14898–906. http://www.sciencedirect.com/science/article/pii/S0360319911004587. [Accessed 5 April 2017].

[18] Chen R, Qi J, Guo J, Schubert P, Hyden J, Taylor EJ. Tolerance of impurities in bioethanol on Pd/C and Pdru/C catalysts toward the ethanol oxidation reaction in alkaline media. 2016. Meet. Abstr. MA2016-01, 1769–1769, http://ma.ecsdl.org/content/MA2016-01/35/1769.short. [Accessed 5 April 2017].

[19] Wang P, Yin S, Wen Y, Tian Z, Wang N. Ternary Pt$_9$RhFe$_x$ nanoscale alloys as highly efficient catalysts with enhanced activity and excellent CO-poisoning tolerance for ethanol oxidation. ACS Appl Mater Interfaces 2017;9(11):9584–91. http://pubs.acs.org/doi/abs/10.1021/acsami.6b14947. [Accessed 5 April 2017].

[20] Yi Q, Niu F, Song L, Liu X, Nie H. Electrochemical activity of novel titanium-supported porous binary Pd-Ru particles for ethanol oxidation in alkaline media. Electroanalysis 2011;23:2232–40. https://doi.org/10.1002/elan.201100148.

[21] Parreira LS, Da Silva JCM, D'Villa -Silva M, Simões FC, Garcia S, Gaubeur I, et al. PtSnNi/C nanoparticle electrocatalysts for the ethanol oxidation reaction: Ni stability study. Electrochim Acta 2013;96:243–52. https://doi.org/10.1016/j.electacta.2013.02.054.

[22] Xu H, Yan B, Zhang K, Wang J, Li S, Wang C, et al. Ultrasonic-assisted synthesis of N-doped graphene-supported binary PdAu nanoflowers for enhanced electro-oxidation of ethylene glycol and glycerol. Electrochim Acta 2017;245:227–36. https://doi.org/10.1016/j.electacta.2017.05.146.

[23] Shafaei Douk A, Saravani H, Noroozifar M. Novel fabrication of PdCu nanostructures decorated on graphene as excellent electrocatalyst toward ethanol oxidation. Int J Hydrogen Energy 2017;42:15149–59. https://doi.org/10.1016/J.IJHYDENE.2017.04.280.

[24] Song G, Yang H, Sun Y, Wang J, Qu W, Zhang Q. Promoting effects of Fe$_2$O$_3$ to Pt electrocatalysts toward methanol oxidation reaction in alkaline electrolyte. J Catal 2017;38(3):554–62. http://www.sciencedirect.com/science/article/pii/S1872206717300219. [Accessed 4 April 2017].

[25] Lović J, Jović V. Electrodeposited Pd and PdNi coatings as electrodes for the electrochemical oxidation of ethanol in alkaline media. J Solid State Electrochem 2017;21(8):2433–41. http://link.springer.com/article/10.1007/s10008-017-3595-2. [Accessed 6 June 2017].

[26] Wang D, Xin H, Hovden R, Wang H, Yu Y, Muller D. Structurally ordered intermetallic platinum–cobalt core–shell nanoparticles with enhanced activity and stability as oxygen reduction electrocatalysts. Nat Mater

2013;12(1):81. http://www.nature.com/nmat/journal/v12/n1/abs/nmat3458.html. [Accessed 2 October 2016].

[27] Cochell T, Manthiram A. Pt@ Pd$_x$Cu$_y$/C core–shell electrocatalysts for oxygen reduction reaction in fuel cells. Langmuir 2012;28(2):1579–87. http://pubs.acs.org/doi/abs/10.1021/la202610z. [Accessed 2 October 2016].

[28] Liu R, Zhou H, Liu J, Yao Y, Huang Z, Fu C. Preparation of Pd/MnO$_2$-reduced graphene oxide nanocomposite for methanol electro-oxidation in alkaline media. Electrochem Commun 2013;26:63–6. http://www.sciencedirect.com/science/article/pii/S1388248112004481. [Accessed 22 September 2016].

[29] Ethanol electro-oxidation in an alkaline medium using Pd/C, Au/C and PdAu/C electrocatalysts prepared by electron beam irradiation. Electrochimica 2013;111:455–65. http://www.sciencedirect.com/science/article/pii/S0013468613015351. [Accessed 18 September 2017].

[30] López-Suárez F, Perez-Cadenas M. Platinum–rhodium–tin/carbon electrocatalysts for ethanol oxidation in acid media: effect of the precursor addition order and the amount of tin. J Appl Electrochem 2015;45(10):1057–68. http://link.springer.com/article/10.1007/s10800-015-0879-z. [Accessed 28 September 2016].

[31] A green method to prepare Pd–Ag nanoparticles supported on reduced graphene oxide and their electrochemical catalysis of methanol and ethanol oxidation. Power Sources 2014;263:13–21. http://www.sciencedirect.com/science/article/pii/S0378775314005096. [Accessed 29 August 2017].

[32] Suffredini H, Tricoli V, Avaca L, Vatistas N. Sol–gel method to prepare active Pt–RuO$_2$ coatings on carbon powder for methanol oxidation. Electrochem Commun 2004;6(10):1025–8. http://www.sciencedirect.com/science/article/pii/S138824810400219X. [Accessed 2 February 2017].

[33] Moura Souza F, Parreira LS, Hammer P, Batista BL, Santos MC. Niobium: a promising Pd co-electrocatalyst for ethanol electrooxidation reactions. J Solid State Electrochem 2017. https://doi.org/10.1007/s10008-017-3802-1.

[34] Figueiredo M, Arán-Ais R, Feliu J, Kontturi K. Pt catalysts modified with Bi: enhancement of the catalytic activity for alcohol oxidation in alkaline media. J Catal 2014. http://www.sciencedirect.com/science/article/pii/S0021951714000207. [Accessed 11 April 2017].

[35] Zhou Y, Zhou H, Karplus M. Cooperativity in Scapharca Dimeric Hemoglobin: Simulation of Binding Intermediates and Elucidation of the Role of Interfacial Water. J Mol Biol 2003;326(2):593–606. https://doi.org/10.1007/BF02904509. Rend Lincei.

[36] Liang ZX, Zhao TS, Xu JB, Zhu LD. Mechanism study of the ethanol oxidation reaction on palladium in alkaline media. Electrochim Acta 2009;54:2203–8. https://doi.org/10.1016/j.electacta.2008.10.034.

[37] Hong J, Kim Y, Wi D, Lee S, Lee S. Ultrathin free-standing ternary-alloy nanosheets. Angew Chem Int Ed 2016. http://onlinelibrary.wiley.com/doi/10.1002/anie.201510460/full. [Accessed 25 May 2017].

[38] Wang A, He X, Lu X, Xu H. Palladium–cobalt nanotube arrays supported on carbon fiber cloth as high-performance flexible electrocatalysts for ethanol oxidation. Angew Chem Int Ed 2015;54(12):3669–73. http://onlinelibrary.wiley.com/doi/10.1002/anie.201410792/full. [Accessed 25 May 2017].

[39] Liang Z, Zhao T, Xu J, Zhu L. Mechanism study of the ethanol oxidation reaction on palladium in alkaline media. Electrochim Acta 2009;54(8):2203–8. http://www.sciencedirect.com/science/article/pii/S0013468608012395. [Accessed 24 May 2017].

[40] Jiang R, Tran DT, McClure JP, Chu D. A class of (Pd-Ni-P) electrocatalysts for the ethanol oxidation reaction in alkaline media. ACS Catal 2014;4:2577–86. https://doi.org/10.1021/cs500462z.

[41] Nagaraju D, Devaraj S, Balaya P. Palladium nanoparticles anchored on graphene nanosheets: methanol, ethanol oxidation reactions and their kinetic studies. Mater Res Bull 2014;60:150–7. Elsevier, http://www.sciencedirect.com/science/article/pii/S0025540814004589. [Accessed 17 December 2017].

[42] Bard AJ, Faulkner LR. Electrochemical Methods: Fundamentals and Applications. 2nd ed. New York: Wiley; 2001. p. 115–24.

[43] Qin Y-H, Li Y, Lam T, Xing Y. Nitrogen-doped carbon-TiO$_2$ composite as support of Pd electrocatalyst for formic acid oxidation. J Power Sources 2015;284:186–93. https://doi.org/10.1016/j.jpowsour.2015.03.040.

[44] PdSn/C electrocatalysts with different atomic ratios for ethanol electro-oxidation in alkaline media. Int J Electrochem 2014;9:5416–24. http://www.electrochemsci.org/papers/vol9/91005416.pdf. [Accessed 29 June 2017].

[45] Zhou ZY, Wang Q, Lin JL, Tian N, Sun SG. In situ FTIR spectroscopic studies of electrooxidation of ethanol on Pd electrode in alkaline media. Electrochim Acta 2010:7995–9. https://doi.org/10.1016/j.electacta.2010.02.071.

[46] Fang X, Wang L, Shen PK, Cui G, Bianchini C. An in situ Fourier transform infrared spectroelectrochemical study on ethanol electrooxidation on Pd in alkaline solution. J Power Sources 2010;195:1375–8. https://doi.org/10.1016/j.jpowsour.2009.09.025.

[47] Neto AO, Nandenha J, Assumpção MHMT, Linardi M, Spinacé EV, de Souza RFB. In situ spectroscopy studies of ethanol oxidation reaction using a single fuel cell/ATR-FTIR setup. Int J Hydrogen Energy 2013;38:10585–91. https://doi.org/10.1016/j.ijhydene.2013.06.026.

[48] Sheng T, Lin WF, Hardacre C, Hu P. Role of water and adsorbed hydroxyls on ethanol electrochemistry on Pd: new mechanism, active centers, and energetics for direct ethanol fuel cell running in alkaline medium. J Phys Chem C 2014;118:5762–72. https://doi.org/10.1021/jp407978h.

[49] Bianchini C, Shen PK. Palladium-based electrocatalysts for alcohol oxidation in half cells and in direct alcohol fuel cells. Chem Rev 2009;109:4183–206. https://doi.org/10.1021/cr9000995.